

# Time-Dependent Transport Through Molecular Junctions

San-Huang Ke,<sup>1</sup> Rui Liu,<sup>2</sup> Weitao Yang,<sup>2</sup> and Harold U. Baranger<sup>3</sup>

<sup>1</sup>Department of Physics, Tongji University, Shanghai 200092, China

<sup>2</sup>Department of Chemistry, Duke University, Durham, North Carolina 27708-0354, USA

<sup>3</sup>Department of Physics, Duke University, Durham, North Carolina 27708-0305, USA

We investigate transport properties of molecular junctions under two types of bias—a short time pulse or an AC bias—by combining a solution for the Green functions in the time domain with electronic structure information coming from *ab initio* density functional calculations. We find that the short time response depends on lead structure, bias voltage, and barrier heights both at the molecule-lead contacts and within molecules. Under a low frequency AC bias, the electron flow either tracks or leads the bias signal (capacitive or resistive response) depending on whether the junction is perfectly conducting or not. For high frequency, the current lags the bias signal due to the kinetic inductance. The transition frequency is an intrinsic property of the junctions.

The goal of achieving the ultimate miniaturization of electronic components is the driving force behind the realization of molecular electronic devices. The idea dates back to at least 1974 [1], and technology has advanced especially rapidly in the last decade [2, 3]. While most nanoscale transport studies have focused on steady state behavior, recently the high frequency (GHz or THz) performance of nanotube and graphene diodes or transistors has been investigated [4–11]. The small junction areas, low capacitances, and high electron mobilities of these molecular devices seem to offer a cutoff frequency in the *THz* range [12]. From the theoretical point of view, the question of how molecules behave under time-dependent perturbation has to be answered since the short time response of functional units is essential to the construction of molecular electronic devices.

In recent years, different theoretical approaches have been developed for this purpose. The methods and schemes employed in these theoretical studies include, for example, time-dependent density functional theory (TDDFT) combined with a Green function technique for open model systems [13], a nonequilibrium Green function (NEGF) method treating the time-dependent bias as a perturbation to the steady-state Hamiltonian [14], real-time TDDFT propagation for closed systems [15, 16], a quantum master equation scheme based on TDDFT for model systems [17], a combination of TDDFT and NEGF with the wide-band limit approximation for open systems [18, 19], real-time propagation of the Kadanoff-Baym equations for open and interacting model systems [20–22], and a self-consistent NEGF formalism for the electron transport through nanotubes under a time-dependent gate potential [23]. Despite the large theoretical effort made by different research groups, the computational studies for real open systems with atomic details described by *ab initio* electronic structure calculations [18, 19, 23] are still lacking because of the computational difficulty.

Within the Keldysh nonequilibrium Green function description [24], Jauho and coworkers have derived formulations of transport in the mesoscopic regime under influence of external time-dependent perturbations. Based on this work, Zhu and coworkers [14] established a computationally efficient method without the need of the wide-band limit (WBL) approximation by using the zero bias equilibrium Green function as the initial state of a tight-binding model system and carrying out

the analysis in the time domain. The finite correlation time in open systems reduces in large part the computational effort and makes this method a practical approach for *ab initio* study.

In the present work, we follow this idea and extend the tight-binding level theory to a density functional theory (DFT) description of the electronic structure, i.e., the initial equilibrium states are obtained by a DFT-Green function formulation [25–29]. We investigate a relatively simple atomic chain system so that we can conveniently adjust various parameters in order to explore the general behavior of molecular junctions under a time-dependent bias, including a short time pulse and an AC bias. In this way, we discuss how the time-dependent transport is affected by the nature of the leads, the lead-molecule coupling, the barrier in the molecule, and the amplitude and frequency of the bias signal.

Following Ref. [14, 24], the time dependent current is

$$I_{\alpha}(t) = \frac{2e}{\hbar} \text{ReTr} \int dt_1 [G^r(t, t_1) \Sigma_{\alpha}^{<}(t_1, t) + G^<(t, t_1) \Sigma_{\alpha}^a(t_1, t)], \quad (1)$$

where  $\Sigma^{</a}(t_1, t)$  is the lesser/advanced self-energy. When no time-dependence is present, the steady state Green function  $\tilde{G}$  is solved by using the NEGF technique in energy space [29]. Under a time-dependent voltage, the single-particle energies become time-dependent in the leads, which causes accumulation and depletion of charges to form a dipole across the device region. Based on the known steady-state Green function  $\tilde{G}$ , we solve for the retarded lesser Green functions by the Dyson and Keldysh equations, respectively [14, 24].

We first investigate the effect of lead structure on the transient response. The system studied is a diatomic hydrogen molecule ( $\text{H}_2$ ) with a 1 Å bond length sandwiched between hydrogen chain leads.

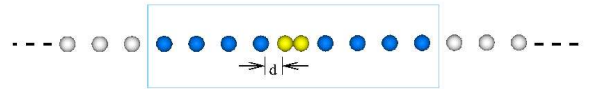


FIG. 1: Illustration of a diatomic hydrogen molecule (yellow) with 1 Å bond length sandwiched between hydrogen chain leads. We vary the interatomic distance in the hydrogen chain but keep the distance between the  $\text{H}_2$  and the leads fixed,  $d = 1.5$  Å. The  $\text{H}_2$  molecule together with four hydrogen atoms on each side form the extended molecule (in the blue box). Bias is applied to the left lead.

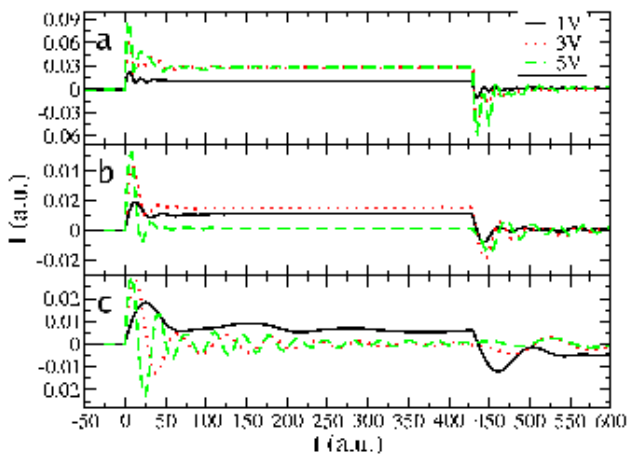


FIG. 2: Current as a function of time (both in atomic units) for the  $H_2$  molecule of Fig. 1 and three different leads: the interatomic distance in the leads is (a) 1.5 Å, (b) 2.0 Å and (c) 2.5 Å. A square shaped voltage pulse is applied to the left lead starting at  $t=0$  and ending at 425. Solid, dotted, and dashed lines correspond to applied voltages of 1, 3, and 5 V, respectively.

two semi-infinite hydrogen chain leads as shown in Fig. 1. The distance from the leads to the  $H_2$  molecule is fixed to be 1.5 Å. We change the H-H distance in the leads, thus varying the interatomic coupling strength. The narrow band width produced by a weak interatomic coupling constrains the electrons, producing less metallic leads.

Single-zeta basis sets (SZ) and optimized Troullier-Martins pseudopotentials [30] are used for all calculations [31]. For hydrogen, if the applied voltage is low so that  $p$  states are not excited, a SZ basis set is a good approximation. The PBE version of the generalized gradient approximation (GGA) functional [32] is adopted for exchange-correlation. For convenience, we adopt atomic units for electric current and time ( $e = \hbar = m_e = 1$ ). An accurate description of atomic and chemical details in the contact region obtained from DFT calculations enables a meaningful study of realistic molecular devices.

The  $I(t)$  characteristics for leads with different H-H distances are shown in Fig. 2. A square shaped voltage pulse is applied to the left lead starting at  $t = 0$  (a.u.) and ending at  $t = 425$ . The time mesh varied between 200 and 600 points for all results shown here; generally, more points were needed for more strongly coupled leads.

The current initially increases for a short time and then oscillates because of interference for several to tens of a.u. depending on the type of leads. We call the time needed for the current to increase from zero to its maximum the finite current response time,  $\tau_R$ . This delay in response is related to the inertia (effective mass) of the carrier and provides a mechanism for inductance (kinetic inductance) different from the magnetic one. As  $\tau_R$  is very short (of order 1 fs), the kinetic inductance is only observable at high frequencies.

The second feature to note in Fig. 2 is that the initial rise in current is steeper when the interatomic distance in the leads is smaller (smaller  $\tau_R$ ) for the same applied voltage. For instance, 1 V bias,  $\tau_R$  is about 4, 10, and 25 for interatomic dis-

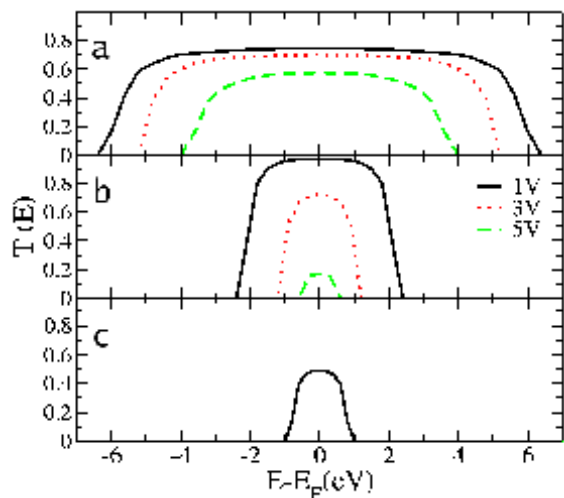


FIG. 3: Transmission as a function of energy for the  $H_2$  molecule of Fig. 1 and the same cases as in Fig. 2. Solid, dotted, and dashed lines correspond to applied voltages of 1, 3, and 5 V, respectively.

tances 1.5, 2.0, and 2.5 Å, respectively. This behavior is easily understood by considering the effective mass of the electrons in these different leads: as the interatomic distance increases, the band width, of course, decreases, and so the electrons have a larger effective mass.

Fig. 2 also shows the relations between bias voltage and the response time. For the leads with wider bands (band width wider than the bias window),  $\tau_R$  is almost independent of the bias (panels a and b), indicating that the kinetic inductance is basically a constant. On the other hand, for the narrow band, less metallic lead (panel c),  $\tau_R$  decreases rapidly for larger bias, showing that the kinetic inductance in this case depends strongly on the magnitude of the bias. One contributing factor is that the electrons are accelerating in the electric field; another is the mismatch between the narrow band in energy on left and that on the right when the bias window is larger than the band width (see Fig. 3 for further discussion). The light might occur, for instance, if a narrow band metallic oxide or silicide is used as the lead material. Over the duration of the transient response, the bias causes alternately accumulating and depleting regions of charge. Subsequently, the current finally tends to a steady state.

In our system, a higher bias does not necessarily lead to a larger steady state current—negative differential conductance can occur. In fact, the possibility of highly nonlinear  $I-V$  curves is one of the appealing features of molecular electronics. Fig. 3 shows the transmission functions,  $T(E)$ , for the same cases as Fig. 2. For reference, the widths of the  $s$ -band in infinite hydrogen chains with interatomic distances 1.5 Å, 2 Å and 2.5 Å are 12.8 eV, 5.7 eV, and 2.4 eV, respectively. Focusing on the case with the narrowest band in the leads (2.5 Å interatomic separation), we see that the net current becomes nearly zero for a bias of 3 V (Fig. 3c). This is because the  $s$ -bands for the left and right leads have no overlap when the bias is greater than the band width, 2.4 eV. Incident electrons encounter a hard wall, causing the current to oscillate over a much longer time than for wide bands. More generally, we

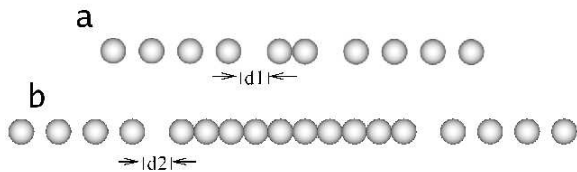


FIG. 4: Schematic of two extended-molecules: (a)  $H_2$  and (b)  $H_{10}$  shown with four atoms of each lead.  $d_1$  and  $d_2$  are the lead-molecule distances.

see that the width of the transmission window equals the difference between the  $s$ -band width and the applied bias.

The discussion in the last paragraph suggests the question: Does a less transparent junction generally lead to a longer time to reach a steady state? To answer this, we vary the barrier height associated with the molecule while keeping all other parameters constant. The barrier height at the molecule-lead contacts can be altered easily by changing the distance between the molecule and the leads. The barrier presented by the molecule itself can be changed by varying the number of atoms. Thus we shall compare results for  $H_2$  and  $H_{10}$  molecules (Fig. 4).

For isolated  $H_2$  and  $H_{10}$  with an interatomic spacing of  $1 \text{ \AA}$ , the gaps between the highest occupied molecular orbital (HOMO) and the lowest unoccupied molecular orbital (LUMO) are  $10.7 \text{ eV}$  and  $3.2 \text{ eV}$ , respectively (DFT GGA calculation). Fig. 4 shows only the extended molecules; note that the bias voltage is applied in the leads, i.e., outside of the extended-molecule region.

Fig. 5 shows the  $I(t)$  curves for both molecules for three values of the lead-molecule separation. The bias voltage applied at  $t = 0$  is not turned off during the simulation. When the molecule-lead coupling is strong ( $d_1 = d_2 = 1.5 \text{ \AA}$ , panel a), both the  $H_2$  and  $H_{10}$  junctions reach steady state quickly,

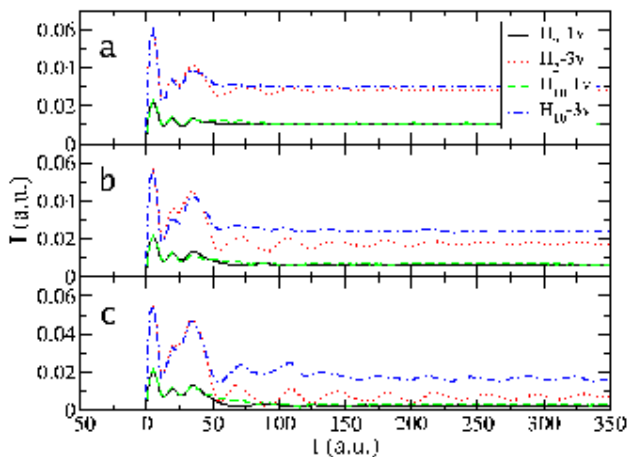


FIG. 5: Current as a function of time for both  $H_2$  and  $H_{10}$  molecules with different coupling strengths to the leads: the molecule-lead distance is (a)  $1.5 \text{ \AA}$ , (b)  $1.7 \text{ \AA}$ , and (c)  $2 \text{ \AA}$ . Results for a bias of both  $1 \text{ V}$  ( $H_2$  solid, and  $H_{10}$  dashed) and  $3 \text{ V}$  ( $H_2$  dotted, and  $H_{10}$  dot-dashed) are shown. The bias is applied at  $t = 0$ ; the interatomic distance in the leads is  $1.5 \text{ \AA}$ .

but note that higher bias causes a longer transient regime. The magnitude of the steady state current is nearly the same for the  $H_2$  and  $H_{10}$  molecules.

When the molecule-lead distance is stretched by  $0.2 \text{ \AA}$  to  $1.7 \text{ \AA}$  (panel b), the low bias behavior of the molecules remains virtually the same, and further there is only modest quantitative change from the strongly coupled case. However, for a  $3 \text{ V}$  bias, the  $I(t)$  curves differ substantially, both from each other and from the previous case. In the short molecule, the duration of the overshoot and oscillating regime is greatly extended, while in the long molecule, there is a surprisingly small decrease in the steady state current ( $2.84 \times 10^{-2}$  in panel a to  $2.25 \times 10^{-2}$  in b).  $H_2$  experiences a more substantial change in current (from  $2.70 \times 10^{-2}$  to  $1.65 \times 10^{-2}$ ) in line with that expected from the fractional change in current at low bias. Thus, the higher molecule-lead barriers are more clearly manifest in the short molecule and hidden in the long one.

These differences are amplified further in the case of largest molecule-lead distance ( $2 \text{ \AA}$ , panel c). The low bias traces are quite similar to each other. At high bias,  $I(t)$  for  $H_2$  oscillates for a long time, while the steady state current for  $H_{10}$  is surprisingly high.

We believe these difference between  $H_2$  and  $H_{10}$  are caused by the larger HOMO-LUMO gap in the short molecule. Fig. 6 shows the projected density of states and transmission functions of both molecules in the weak coupling case (molecule-lead separation of  $2 \text{ \AA}$ ). The  $T(E)$  within the bias window for a  $1 \text{ V}$  bias (i.e.  $-0.5 \text{ V}$  to  $0.5 \text{ V}$ ) are almost identical for  $H_2$  and  $H_{10}$ . In contrast, for a  $3 \text{ V}$  bias, the  $T(E)$  within the bias window, now  $-1.5 \text{ V}$  to  $1.5 \text{ V}$ , are totally different: for  $H_{10}$ , the tails of two resonant peaks extend into the bias window. Therefore the long molecule is much more transparent, leading to a larger current flow and less oscillatory behavior compared to the short molecule. Thus we see that both molecule-lead barriers and internal barriers within the molecules can cause significant changes in the  $I(t)$  characteristics.

After studying the transient response to a square shaped

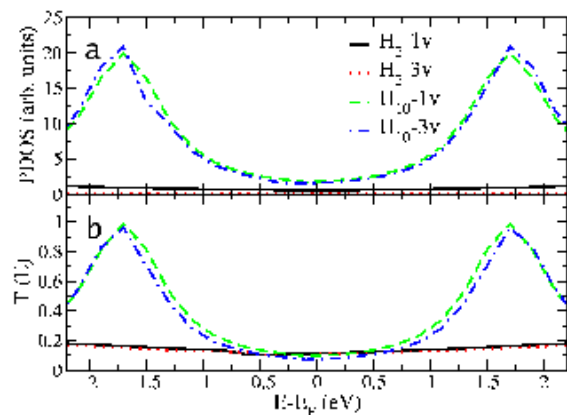


FIG. 6: Projected density of states and transmission functions for both the long and short molecules connected to hydrogen chain leads ( $1.5 \text{ \AA}$  interatomic distance). The molecule-lead distance is fixed at  $2 \text{ \AA}$ . At energies more than  $1 \text{ eV}$  away from  $E_F$ , the properties of  $H_2$  molecular junctions ( $1 \text{ V}$  solid,  $3 \text{ V}$  dotted) differ greatly from those of  $H_{10}$  ( $1 \text{ V}$  dashed,  $3 \text{ V}$  dot-dashed).

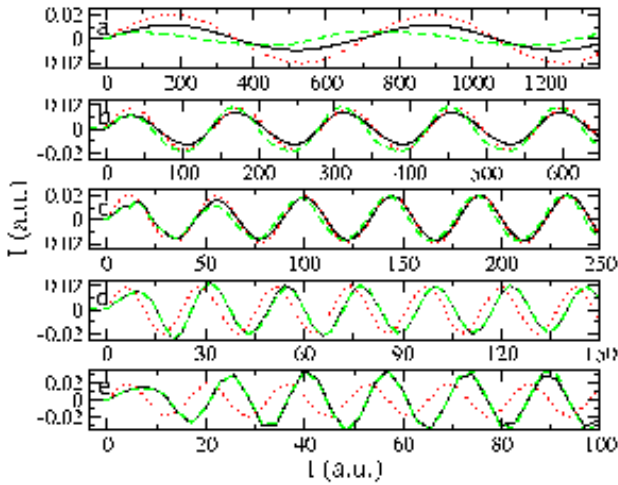


FIG. 7: Current as a function of time for  $H_2$  molecules subjected to AC signals of varying frequencies, smaller to higher from panel a to e. A well-coupled case (solid,  $d1 = 1.5 \text{ \AA}$ ) and weakly-coupled case (dashed,  $d1 = 2 \text{ \AA}$ ) are compared to the applied voltage (dotted, 1 V amplitude). The interatomic distance in the leads is  $1.5 \text{ \AA}$ .

pulse, we now look at how a molecular junction acts when a sinusoidal voltage with period  $T$  is applied. The frequency should be slower than the plasma frequency  $\omega_P$  of the leads so that the electric field is effectively screened and the voltage drops across the device region. For most metals, the plasma frequency is in the ultraviolet regime, ranging from  $10^{15}$  Hz to  $10^{17}$  Hz, so typically this criterion is satisfied. For the 1D hydrogen chains in our calculations,  $\omega_P$  is of order  $10^{17}$  Hz, assuming the dielectric constant and permeability are that of vacuum and the length of the device is around 1 nm [33].

Fig. 7 shows the AC response of  $H_2$  junctions (schematic in Fig. 1) with two molecule-lead distances, 1.5 and 2  $\text{\AA}$ , representing the well-coupled and weakly-coupled regime, respectively. First, consider the low frequency cases,  $T/4 \gg \tau_R$  (panels a, b, and c). The current response of the well-coupled system tracks the sinusoidal signal, while for the weakly coupled junction, the current leads the bias voltage. This behavior can be understood by considering the equivalent electric circuit of the lead-molecule-lead system. At low frequency, the inductance is not important, so we ignore it temporarily; then we can view the junctions as a resistor ( $R$ ) and capacitor ( $C$ ) in parallel formed by the two contact interfaces. For the well-coupled system ( $d1 = 1.5 \text{ \AA}$ ), there is actually no interface, and thus the capacitor disappears, and the whole system is basically resistive. When the coupling is weaker, the capacitor is formed, making the system capacitive in nature.

As the frequency increases, the kinetic inductance gradually appears; consequently, the phase shift of the weakly-coupled system becomes progressively smaller in panels a, b, and c of Fig. 7. As the frequency increases further,  $T/4$  becomes shorter, approaching the finite current response time  $\tau_R$ . Then the effect of the delay in current becomes significant and at a certain frequency the characteristics of the junction changes from capacitive to inductive, as shown in panel d. Our results are qualitatively consistent with a recent calculation for an Al-nanotube-Al junction where it was found

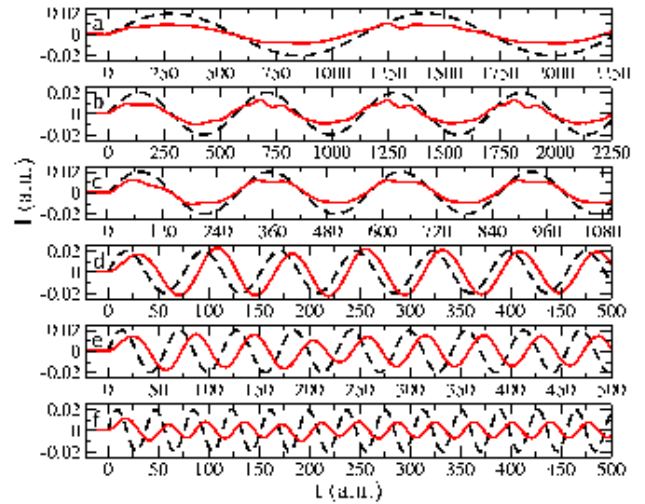


FIG. 8: Current as a function of time (solid) for  $H_2$  molecules subjected to AC signals (dashed) of varying frequencies, smaller to higher from panel a to f. The molecule-lead distance  $d1$  equals  $1.5 \text{ \AA}$ , and the interatomic distance in the leads is  $2.5 \text{ \AA}$ .

that the system is inductive for a high bias frequency ( $T \sim$  response time) [19].

To support our explanation, we consider different values of  $\tau_R$ . Since we showed that  $\tau_R$  in 1D molecular junctions is significantly affected by the nature of the leads, we consider a different lead structure but keep the intramolecular and lead-molecule structure the same. Thus the lead-molecule separation ( $1.5 \text{ \AA}$ ) becomes different from the interatomic distance ( $2.5 \text{ \AA}$ ) in the leads, and therefore a capacitor is formed. The  $I(t)$  curves in Fig. 8 show that the current now leads the bias even for very small frequency (panels a and b). The current response changes, as expected, from capacitive to inductive as the bias frequency increases; however, compared to the system with  $1.5 \text{ \AA}$  interatomic distance, the transition frequency decreases from  $2.8 \times 10^{-2}$  (Fig. 7d) to  $3.6 \times 10^{-3}$  (Fig. 8c). This reduction is consistent with the change in  $\tau_R$ : As the interatomic distance in the leads becomes larger,  $\tau_R$  increases from  $\sim 4$  to  $\sim 25$  (Fig. 7 a and c). As a caution, we mention that since the intrinsic magnetic inductance has not been taken into account here, the total inductance of the 1D molecular junctions may be underestimated; however, the magnetic inductance may be much smaller than the kinetic one for high frequencies (THz) [8, 34–38].

It is interesting to note that the magnitude of the current driven by an AC bias is not necessarily consistent with that driven by a DC bias. In Fig. 5, the current through  $H_2$  with  $d1 = 2.0 \text{ \AA}$  is smaller than that with  $d1 = 1.5 \text{ \AA}$ . This is because the contact barrier in the former is higher. In contrast, under a high-frequency AC bias, the magnitudes of the current in these two cases become very close, as shown in Fig. 7. Although both bias frequencies are much slower than the plasma frequency  $\omega_P$ , the time needed for the system to reach its steady state is much longer, by orders of magnitude, than  $1/\omega_P$  due to the very weak screening in the 1-D structure. Only when  $T/4$  of the AC bias is much longer than this time does the

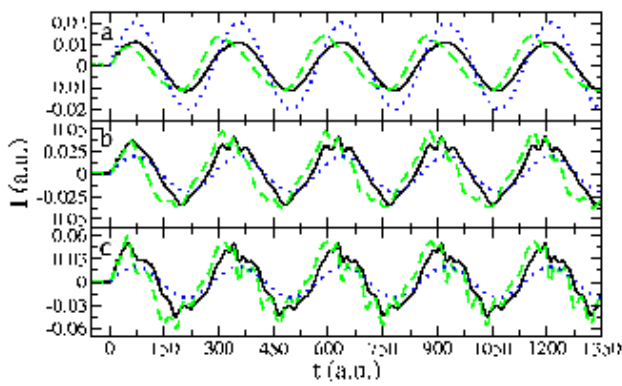


FIG. 9: Current as a function of time for  $H_2$  molecules subjected to AC signals of different magnitude: 1 V, 3 V, and 5 V for panels a, b, and c, respectively.  $I(t)$  for two lead-molecule spacings are shown,  $d_1 = 1.5 \text{ \AA}$  (solid) and  $2 \text{ \AA}$  (dashed), and compared to the applied voltage (dotted). The interatomic distance in the leads is  $1.5 \text{ \AA}$ .

AC current reflect the steady state current; otherwise, it will largely be determined by the transient states. Because the transient states are determined by the *extended molecule* instead of the molecule and the contact alone, the magnitude of the

AC current can be very different from that of the DC current in the same system.

Finally, we point out that when the AC frequency is relatively small, irregular behavior can be significant, as we saw for pulsed signals. We show in Fig. 9 that as the voltage magnitude increases (from 1 V to 5 V), the current response may not follow a sinusoidal wave. The irregular features are larger when the junction is less transparent. This is in line with our previous conclusion (Fig. 2c) and applies to the situation of relative low frequency AC response.

In conclusion, the transient response of a molecular junction depends on the lead structure, bias voltage, and barrier height seen by the transported electrons. A higher electron density or a smaller effective mass leads to a faster response characterized by a smaller current response time  $\tau_R$ . A high barrier height yields long oscillatory behavior in current, seen in both the pulsed and AC situations. The current follows the AC signal only when a junction is perfectly conducting and the signal frequency is slow ( $T/4 \gg \tau_R$ ); otherwise, a lead-molecule-lead junction should be viewed as a complex circuit consisting resistors, capacitors, and inductors. Currents can lead or lag the AC signal, and the transition frequency between the two regimes is an intrinsic property of the junction.

- 
- [1] A. Aviram and M. R. Ratner, Chem. Phys. Lett. **29**, 277 (1974).  
 [2] A. Nitzan and M. A. Ratner, Science **300**, 1384 (2003).  
 [3] N. J. Tao, Nature Nano. **1**, 173 (2006).  
 [4] S. Li, Z. Yu, S.-F. Yen, W. C. Tang, and P. J. Burke, Nano Lett. **4**, 753 (2004).  
 [5] H. M. Manohara, E. W. Wong, E. Schlecht, B. D. Hunt, and P. H. Siegel, Nano Lett. **5**, 1469 (2005).  
 [6] S. Rosenblatt, H. Lin, V. Sazonova, S. Tiwari, and P. L. McEuen, Appl. Phys. Lett. **87**, 153111 (2005).  
 [7] J. Guo, S. Hasan, A. Javey, and G. Bosman, IEEE Trans. Nanotechnol. **4**, 715 (2005).  
 [8] J. J. Plombon, K. P. O'Brien, F. Gstrein, V. M. Dubin, and Y. Jiao, Appl. Phys. Lett. **90**, 063106 (2007).  
 [9] L. Gomet-Rojas, S. Bhattacharyya, E. Mendoza, D. C. Cox, J. M. Rosolen, and S. R. P. Silva, Nano Lett. **7**, 2672 (2007).  
 [10] J. Chaste, L. Lechner, P. Morfin, G. Feve, T. Kontos, J.-M. Berroir, D. C. Glattli, H. Happy, P. Hakonen, and B. Placais, Nano Lett. **8**, 525 (2008).  
 [11] Y.-M. Lin, K. A. Jenkins, A. Valdes-Garcia, J. P. Small, D. B. Farmer, and P. Avouris, Nano Lett. **9**, 422 (2009).  
 [12] P. J. Burke, Solid-State Electron **48**, 1981 (2004).  
 [13] S. Kurth, G. Stefanucci, C.-O. Almbladh, A. Rubio, and E. K. Gross, Phys. Rev. B **72**, 035308 (2005).  
 [14] Y. Zhu, J. Maciejko, T. Ji, and H. Guo, Phys. Rev. B **71**, 075317 (2005).  
 [15] C.-L. Cheng, J. S. Evans, and T. V. Voorhis, Phys. Rev. B **74**, 155112 (2006).  
 [16] N. Sai, N. Bushong, R. Hatcher, and M. D. Ventra, Phys. Rev. B **75**, 115410 (2007).  
 [17] X.-Q. Li and Y.-J. Yan, Phys. Rev. B **75**, 075114 (2007).  
 [18] X. Zheng, F. Wang, C. Y. Yam, Y. Mo, and G. Chen, Phys. Rev. B **75**, 195127 (2007).  
 [19] C. Yam, Y. Mo, F. Wang, X. Li, G. Chen, X. Zheng, Y. Matsuda, J. Tahir-Kheli, and W. A. G. III, nt **19**, 495203 (2008).  
 [20] P. Myohanen, A. Stan, G. Stefanucci, and R. V. Leeuwen, Europhys. Lett. **84**, 67001 (2008).  
 [21] A. Prociuk and B. D. Dunietz, Phys. Rev. B **78**, 165112 (2008).  
 [22] P. Myohanen, A. Stan, G. Stefanucci, and R. V. Leeuwen, Phys. Rev. B **80**, 115107 (2009).  
 [23] D. Kienle and F. Leonard, Phys. Rev. Lett. **103**, 026601 (2009).  
 [24] A. P. Jauho, N. S. Wingreen, and Y. Meir, Phys. Rev. B **50**, 5528 (1994).  
 [25] P. S. Damle, A. W. Ghosh, and S. Datta, Phys. Rev. B **64**, 201403 (2001).  
 [26] Y. Xue, S. Datta, and M. A. Ratner, Chem. Phys **281**, 151 (2002).  
 [27] M. Brandbyge, J. L. Mozos, P. Ordejón, J. Taylor, and K. Stokbro, Phys. Rev. B **65**, 165401 (2002).  
 [28] J. Taylor, H. Guo, and J. Wang, Phys. Rev. B **63**, 245407 (2003).  
 [29] S. H. Ke, H. U. Baranger, and W. Yang, Phys. Rev. B **70**, 085410 (2004).  
 [30] M. Troullier and J. L. Martins, Phys. Rev. B **43**, 1993 (1991).  
 [31] J. M. Soler, E. Artacho, J. D. Gale, A. García, J. Junquera, P. Ordejón, and D. Sánchez-Portal, J. Phys.: Condens. Matter **14**, 2745 (2002).  
 [32] J. P. Perdew, K. Burke, and M. Ernzerhof, Phys. Rev. Lett. **77**, 3865 (1996).  
 [33] J. Wang and J. P. Leburton, Phys. Rev. B **41**, 7846 (1989).  
 [34] P. J. Burke, IEEE Trans. Nanotechnol. **2**, 55 (2003).  
 [35] S. Li, Z. Yu, S. F. Yen, W. C. Tang, and P. J. Burke, Nano Lett. **4**, 753 (2004).  
 [36] Z. Yu and P. J. Burke, Nano Lett. **5**, 1403 (2005).  
 [37] S. Rosenblatt, H. Lin, V. Sazonova, S. Tiwari, and P. L. McEuen, Appl. Phys. Lett. **87**, 153111 (2005).  
 [38] M. Shang, X. Huo, P. C. H. Chan, Q. Liang, and Z. K. Tang, IEEE Electron Device Lett. **27**, 668 (2006).